Nanostructured Ni-Co Alloy Electrodes for both Hydrogen and Oxygen Evolution Reaction in Alkaline Electrolyzer

Fabrizio Ganci*, Valentino Cusumano, Patrizia Livreri, Giuseppe Aiello, Carmelo Sunseri, Rosalinda Inguanta

Dipartimento di Ingegneria

Università di Palermo, Viale delle Scienze, 90128 Palermo (Italy)

e–mail: fabrizio.ganci@unipa.it

ABSTRACT

Ni-Co alloy nanostructured electrodes with high surface area were investigated both as a cathode and anode for an alkaline electrolyzer. Electrodes were obtained by template electrosynthesis at room temperature. The electrolyte composition was tuned in order to obtain different NiCo alloys. The chemical and morphological features of nanostructured electrodes were evaluated by EDS, XRD and SEM analyses. Results show that electrodes with different composition of Ni and Co, made of nanowires well anchored to the substrate, were obtained. For both hydrogen and oxygen evolution reactions, electrochemical and electrocatalytic tests, performed in 30% w/w KOH aqueous solution, were carried out to establishing the best alloy composition. Mid-term tests conducted at a constant current density were also reported. Results show that nanostructured electrodes with a Co atomic composition of 94.73% have the best performances for both hydrogen and oxygen evolution reactions. In particular, with this alloy, a potential of -0.43 V(RHE) and of 1.615 V(RHE) was measured for

* Corresponding author

hydrogen and oxygen evolution reaction at -50 $mAcm^{-2}$ and at 50 $mAcm^{-2}$, respectively, after 6h of electrolysis ~~at 50 $mAcm^{-2}$~~. The calculated Tafel slopes for HER and OER were -0.105 and 0.088 V/dec, respectively. Furthermore, HER and OER η_{10} potential values were measured founding -0.231 V(RHE) and 1.494 V(RHE) respectively.

KEYWORDS: Alkaline Electrolyzer, Nanostructured Electrodes, Ni-Co Alloy, HER, OER, Template Electrosynthesis.

1 INTRODUCTION

The consumption of fossil fuels for the production of primary energy is the main cause of the increasing concentration of greenhouse gases in the atmosphere. One of the possible solutions to reduce this consumption is the exploitation of renewable sources [1]. However, the intrinsic randomness of the renewable sources requires their coupling with storage energy systems [2]. Among them, hydrogen produced by electrolysis is one of the most promising and environmentally sustainable method [3-5]. Nevertheless, the electrochemical water splitting is not yet economically competitive compared to other hydrogen production methods due to the high electrical energy required by the hydrolysis [6, 7]. Among the three technologies (Alkaline, Proton exchange membrane and Solid Oxide electrolyzer), Alkaline Electrolyzer (AE) is the widely used for large-scale applications due its simplicity and relative low cost compared to the other ones [8]. However, this technology still has some limitations such as durability, maintenance cost, low operating current density and pressure (the lower among the electrolyzers), and high price of the produced hydrogen. Besides, AE is not suitable to work in dynamic operation (frequent start-ups and varying power supply) because this mode decreases

both efficiency and purity of produced gas. This is a very important limitation because the dynamic operation would allow the use of AE with intermittent renewable sources [9].

Different efforts have been made to overcome these issues. In particular, the attention has been focused on the development of new materials, such as nanostructured materials, in order to improve the electrocatalysis and therefore reduce energy losses [10]. To be competitive with the other technologies, these materials must have excellent electrocatalytic activity for both hydrogen (HER) and oxygen evolution reaction (OER), high active surface area and electrical conductivity, proper chemical stability and cost effectiveness. Consequently, very different materials were proposed as electrocatalysts for AE [11]. For OER, transition metal oxides (Ni, Co, Fe, Mn) are the most studied because their stability, high activity at high pH value, and low-cost due to their abundancy [12, 13]. As proposed by Bockris [14], the high activity of these materials is due to number of d electrons. Ni is the most efficient, and it has been also demonstrated that combining Ni with Co or Fe significant improvements in the electrode performance were obtained, owing to reduced charge transfer overpotential losses [15, 16]. Metal oxides have the disadvantages of low electrical conductivity that can be partly overcome by incorporation of carbon nanotubes [17]. Also, metal-free carbon nanotubes and perovskites, with structure of ABO_3, were proposed [18, 19].

In the case of HER, the most typical electrocatalyst in alkaline media is based on transition metal oxides [20]. In particular, Ni is the most used, owing to its low cost and high chemical stability in alkaline environment even if it is subjected to deactivation phenomena (Ni fresh cathodes have an activity significantly greater than the same electrodes after long-term continuous operation) [21]. The deactivation of Ni was attributed to the formation of nickel hydride, but it was demonstrated that alloying nickel with other metals is useful to prevent the formation of this phase and improve electrode stability [22]. Among nickel alloys, NiCo [23] and NiPd [24, 25] were proposed as the most promising. As showed by Hong et al. [26], NiCo alloys exhibit

improved activity compared with pure Ni and Co electrocatalysts. Alternative to metals for HER in alkaline environments, silicides [27] and nitrides [28] were also suggested.

Apart the good electrocatalytic behaviour and high chemical stability in alkaline media, NiCo alloys have also other interesting properties. In fact, as reported in Karimhazed et al. [29], due to good magnetic properties, NiCo electrodeposited coatings are used in computer technology for chips and hard drives production and in microelectromechanical systems (MEMS). Besides, due to mechanical resistance, these materials are widely used for high-temperature applications.

In recent years, in order to further improve the efficiency and/or reduce the catalysts loading, especially of precious metals, nanostructured morphology has gained considerable attention [30]. Electrocatalyst with nanostructured morphology has large surface area, good electronic conductivity, satisfying porosity, and guarantees detachment of gas bubbles from the surface, which in turn affects the availability of active sites [31]. For example, Wang et al. [32] have developed NiCo oxide nanostructures with high surface area having a low charge transfer overpotential of 0.34 V at 10 mA cm^{-2}, while Au/$NiCo_2O_4$ nanoarrays exhibited good activity and high stability for OER in the alkaline environment [33]. $NiCoO_4$ nanoplatelets were developed by Cui et al. [34], obtaining enhanced performance, compared to bulk $NiCoO_4$ and Co_3O_4. For HER in alkaline solution, Ni foam with deposited Pd and Ru nanoparticles was tested, obtaining improvement of catalytic activity in comparison with un-coated foam [35]. RuO_2–NiO nanorod arrays on a Ni foam showed small charge transfer resistance, excellent HER performance and long-term stability [36]. Recently, it was also proved that ternary Ni-Fe-Co alloy with a nanocone morphology, obtained by electrodeposition, exhibits excellent properties, with an overpotentials of 91 mV and 316 mV for the evolution of H_2 and O_2 respectively, at a current density of 10 mA cm^{-2} [37]. It was also demonstrated that [38] amorphous NiCoP, deposited on nickel nanocone array using cyclic voltammetry, exhibits low overpotential and remarkable electrochemical stability.

In this work, starting from above data and the previous good results obtained in the case of the nanostructured electrodes of Ni [39], Ni-IrO_2 [40], and Ni/Pd [24, 41], we have studied the performance of Ni-Co alloy nanostructured electrodes obtained by electrodeposition into nanoporous template. In particular, nanostructured electrodes made of nanowires (NWs) with a surface area about 70 times higher the geometrical one [42] were obtained. Deposition solutions with various Ni and Co concentrations were used to obtain alloys with different compositions. For a better comparison between the alloys and to evaluate effective improvement in their use, pure Ni and Co nanostructured electrodes were also fabricated. Electrochemical and electrocatalytic characterization were carried out to estimate the properties of nanostructured alloys for both HER and OER in alkaline electrolyte. In addition, in order to simulate the operation in electrolyzer, the electrodes were tested at constant current density for 6 hours.

2 MATERIALS AND METHODS

2.1 Electrode fabrication.

Polycarbonate nanoporous membranes (Whatman), with a mean pore diameter of 200 nm and a thickness of about 20 mm, were employed as a template for electrode fabrication. The Ni deposition solution was a typical Watt's bath (300 g/L nickel sulphate hexahydrate, 45 g/L nickel chloride, 45 g/L boric acid, at pH 3). For Co electrodeposition the electrolyte was made with 300 g/L cobalt sulphate heptahydrate, 45 g/L cobalt chloride, and 45 g/L boric acid. The solution pH was pH 3. The procedure for NWs fabrication was detailed by Ganci et al. [24, 41]. Briefly, after deposition of a very thin gold film (only on one side of the template), a layer of either Ni or Co was electrodeposited (in potentiostatic mode at -1.5 V vs. SCE, with a deposition time of 9000 s) in order to obtain a current collector and a mechanical support of nanostructures. Nanowires were obtained by pulsed potential electrodeposition into the

template nanochannels using the same potential wave proposed in [24, 41]. In particular, the potential was scanned between -0.3 and -1.25 V vs. SCE for 90 times with a scan rate of 0.1 Vs^{-1}. The lower value of applied potential was chosen in order to avoid the formation of nanotubes due to the concurrent hydrogen evolution reaction. A standard tree electrode cell was used with a Pt mesh as a counter electrode and a saturated calomel electrode as a reference (0.242 V vs SHE). The area of working electrode was 10.75 cm^2. Different nanostructured electrodes were obtained by tuning the concentration of Ni and Co in the electrodeposition bath. In particular, starting from the solutions composed exclusively of Ni and Co, electrolytes with variable composition have been obtained by mixing different volumes of them. In Table 1, the composition of the final employed solutions was reported. For each experiment a fresh solution was used and the deposition was carried out at room temperature. After deposition, the template was etched in dichloromethane at room temperature. To ensure the total removal of the polycarbonate the etching was repeated 4 times using fresh solvent for each step.

2.2 Electrode Characterization.

A FEG-ESEM microscope (model: QUANTA 200 by FEI), equipped with Energy Dispersive Spectroscopy (EDS) probe, was used to investigate the morphology and the atomic composition of nanostructured electrode. EDS analyses were carried out on both current collector (CC) and NWs side in order to evaluate possible difference on composition. Besides, different areas of samples were exanimated in order to investigate the uniform composition of NWs. XRD analyses were carried out with a RIGAKU X-ray diffractometer (model: D-MAX 25600 HK). Diffraction patterns were obtained in the 2θ range from 20° to 80° with a sampling width of 0.01° and a scan speed of 4.00 °/min, using Ni-filtered Cu Kα radiation (λ= 1.54 Å). The tube voltage and current were set at 40 kV and 40 mA, respectively. The

identification of phases was performed by comparison with the literature data. Electrochemical and electrocatalytic tests were carried out in KOH 30% w/w aqueous solution using a tree electrode cell. As counter-electrode, a Ni sheet (with a surface area of about 20 cm^2) was employed. An Hg/HgO reference electrode was employed, although in the following, all potentials will be referred to the value of reversible hydrogen electrode (RHE) at pH 14. All electrodes were characterized by cyclovoltammetry (CV) and quasi-steady-state polarization (QSSP). CV curves were measured in the potential range from -0.035 V(RHE) to 1.265 V(RHE) with a scan rate of 0.005 Vs^{-1}. For QSSP curves, the scanned potential range was 1 V at scan rate of 0.1667 mVs^{-1}; for HER the potential range was scanned from 0.1 V(RHE) to -0.9 V(RHE), while for OER it was scanned from 1.1 V to 2.1 V vs. RHE. The electrochemical tests were carried out at room temperature.

The nanostructured electrodes were also subjected to constant current density tests to evaluate their mid-term behaviour. Before electrochemical tests, the electrodes were insulated in order to limit a geometrical area of about 0.5 cm^2.

All experiments were performed using a Cell Test System (Solartron, Mod. 1470 E). Data were recorded by MultiStat Software. Each experiment reported in this work was repeated at last three times.

3 RESULTS AND DISCUSSUION

3.1 Electrode fabrication.

Nanostructured electrodes with different composition were obtained by tuning the composition of the electrodeposition bath. Pure Ni and Co nanostructured electrode were also fabricated in order to compare their performance with respect to NiCo alloys. Pure Ni and Co NWs were obtained in a current collector of Ni and Co, respectively, while NWs alloys were

fabricated on a current collector with a similar alloy composition. After electrodeposition and membrane dissolution, EDS analysis was performed to evaluate the electrode composition. Figure 1 shows two typical EDS spectra of electrodes with low (Fig. 1a) and high (Fig. 1b) Co content. It can be observed that, the presence of only Ni and Co peaks were revealed, with different relative intensity due to different composition of the sample. The analysis was carried out on both Current Collector (CC) and NWs side in order to evaluate possible differences in the composition. Different areas of samples were exanimated in order to investigate the uniform composition of NWs. A mean value of atomic composition was calculated and the results are summarized in Table 1.

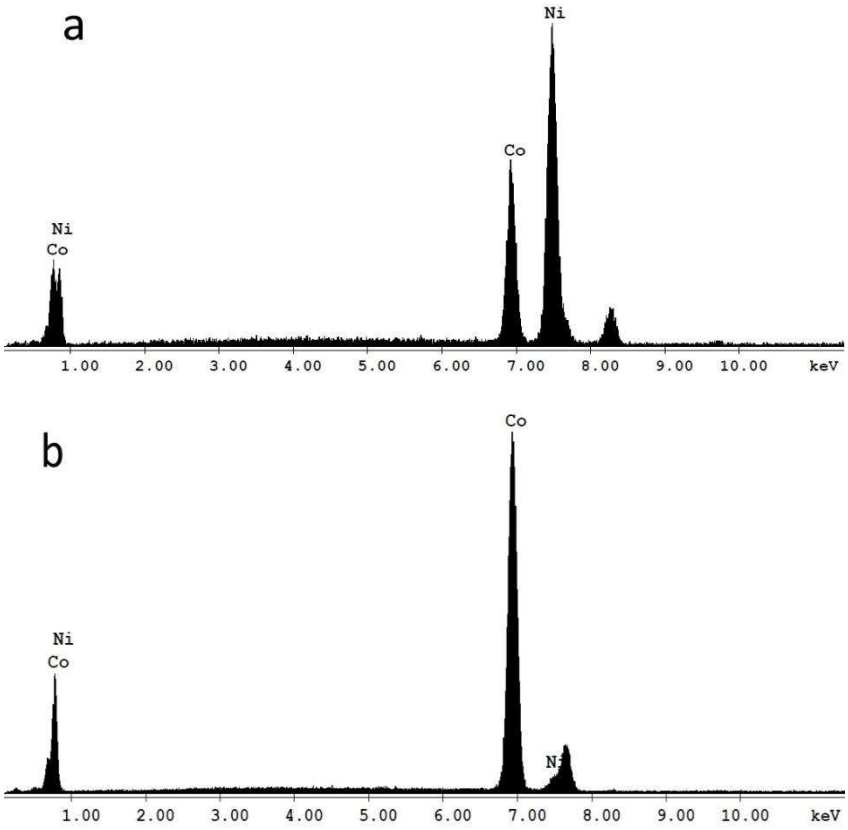

Figure 1. EDS patterns of Ni-Co alloy NWs: (a) low Co composition (32.45%), (b) high Co composition (94.73%).

In Table 1, it is possible to compare the composition of the alloy and cobalt content in the electrolyte. Besides, Figure 2 shows the atomic composition of Co in the nanostructured alloy as a function of Co concentration in the deposition bath. In agreement with analogous findings on deposited Co alloys, the curve of Figure 2 together with the data reported in Table 1 show that the Co content is higher in the alloy than in the electrolyte [43, 44].

Table 1. Current Collector (CC) and NWs atomic composition

Solution concentration V/V (%)	CC composition (%)		NWs composition (%)	
	Ni	Co	Ni	Co
Ni 100 - Co 0	100	0	100	0
Ni 95 - Co 5	80.39	19.61	67.55	32.45
Ni 90 - Co 10	68.92	31.08	52.15	47.85
Ni 84 - Co 16	55.20	44.80	33.87	66.13
Ni 66 - Co 34	20.82	79.18	14.94	85.06
Ni 50 - Co 50	9.89	90.11	7.54	92.46
Ni 34 - Co 66	4.61	95.39	5.26	94.73
Ni 16 - Co 84	2.74	97.26	2.19	97.81
Ni 0 - Co 100	0	100	0	100

This finding can be due to both the specific ligand role of the boric acid in solution towards Ni ions [45] and to kinetics of electrodeposition. In particular, although the standard electrochemical potential of Ni^{2+}/Ni (−0.257 V/NHE) is slightly higher than that one of Co^{2+}/Co (−0.277 V/NHE), the stability constant of Ni-Borate complex is higher than Co-Borate complex [46]. Consequently, in electrodeposition bath containing both complexes the reduction of Ni^{2+} becomes less favoured. Thus, a Co enrichment of the alloy can be explained assuming that Co^{2+} deposition is faster than Ni^{2+} reduction and its charge transfer overpotential lowers with increasing Co content in the alloy. In addition, it is also evident the different composition of the current collector (more similar to the solution concentration) with respect to the NWs. This is due to both the different electrodeposition technique used [47] (for current collector is current constant deposition, while for the NWs is a pulsed potential

deposition) and to the confined ambient of NWs deposition (inside the nanopores of template), where electrochemical conditions are quite different from those usually established for deposition on a flat substrate [48].

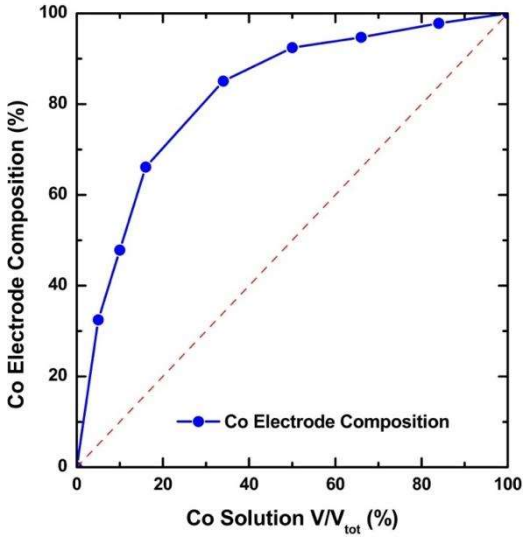

Figure 2. NiCo NWs composition as a function of Co concentration in the electrodeposition bath.

The XRD patterns of the samples are shown in Figure 3. In the case of pure Co electrodes, the peaks of ε-Co phase with a hexagonal close-packed (hcp) lattice can be seen. For pure Ni, the peaks are relative to well crystalline α-Ni with face-centered cubic (fcc) structure (ICDD® (International centre of diffraction data) card no. 04-850). In this pattern, the peak located at about 40° is unknown and it is probably imputable to native oxide of Ni. With the decrease of Co/Ni ratio, the ε-Co (hcp, ICDD® no. 05-0727) peak at 41.6 shifts towards high 2θ values, besides a contemporary decrease of its intensity can be observed. With the increase of Ni content (see pattern of Co32.45 sample) the characteristic peak of α-Ni and/or α-Co (face-centered cubic (fcc); ICDD®15-0806) appears. These data agree with those reported in the literature [49, 50] where, for alloys rich in Co, the most reported phase is the hcp, while alloys

with higher Ni content exhibit fcc peaks of α-Ni and α-Co fcc lattice. Besides, samples that contain Co are characterized by a nanocrystalline nature, in particular the alloy with about 95% of cobalt, and in fact almost wide peaks with very low intensity, in comparison to that of Ni, were measured. The nanocrystalline (almost amorphous) nature is a characteristic of Co and its alloys [51].

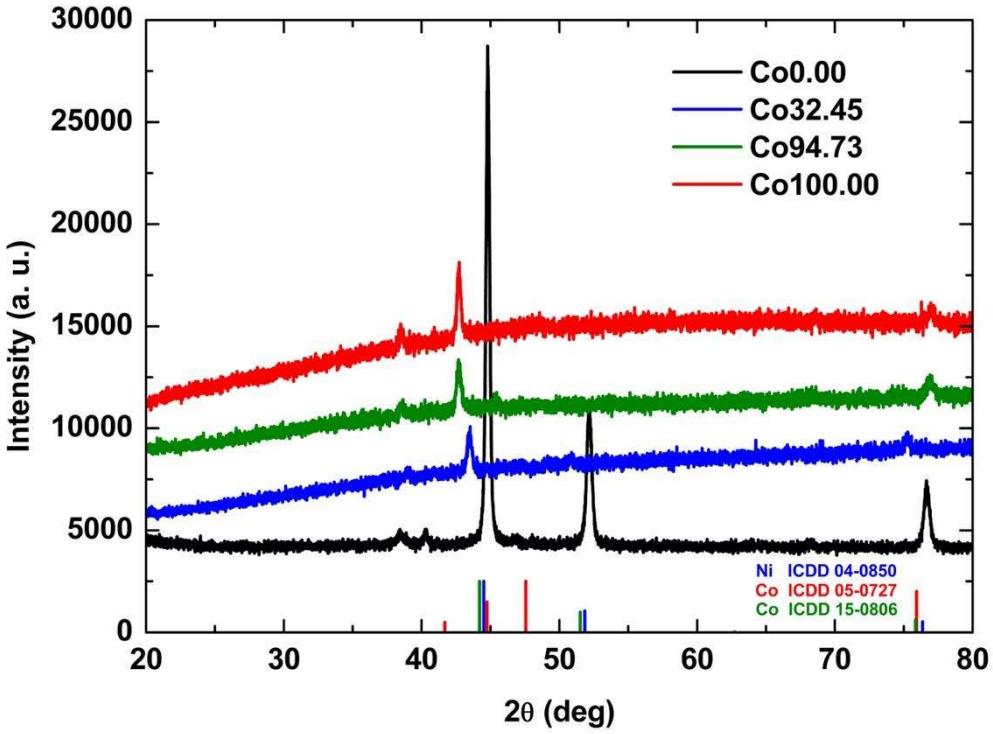

Figure 3. XRD patterns of Ni, Co, and NiCo alloys NWs (the ICDD data used to identify the different phases were also reported).

In Figure 4, typical SEM images of Ni-Co NWs are shown at two different magnifications. NWs cover completely the current collector (Figure 4a), have a cylindrical shape and are highly interconnected (Figure 4b), conformal to the template. As can be observed in Figure 4a, they are also well adherent to the current collector. A diameter of about 220-250 nm and a length of about 5-6 μm was measured. The NWs surface appears smooth and without irregularities. It is

important to emphasize that the NWs morphology does not depend on either the electrode or electrolyte composition (Figure S1).

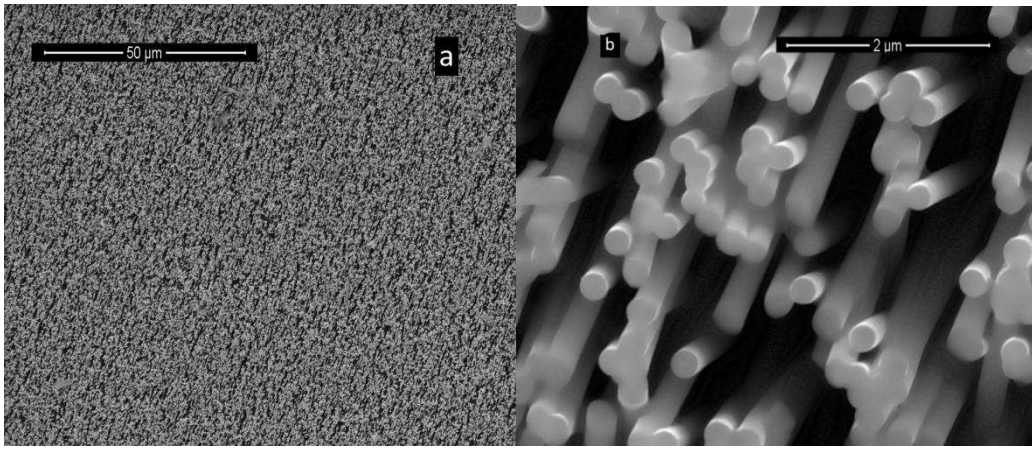

Figure 4. SEM images of Ni-Co alloy NWs with a composition of Co66.13.

As reported in [52], this type of nanostructured morphology ensures the improvement of electrocatalytic activity of the electrode. This behaviour is attributable to the super aerophobic surface, that led to a rapid separation of gas bubbles formed on the surface [53], which in turn affects the availability of active sites [31].

3.2 Electrode Characterization.

In order to evaluate the electrochemical and electrocatalytic electrode behaviour, cyclic voltammetry (CV), quasi steady-state polarization (QSSP) and galvanostatic polarization were carried out. In this work, the results reported below refer to electrodes with four different composition, considered the most relevant for the purposes of the discussion. In particular, the electrodes that have been tested are: i) pure Ni NWs (Co0.00), ii) poor Co alloy NWs (Co32.45), iii) rich Co alloy NWs (Co94.73), iv) pure Co NWs (Co100.00).

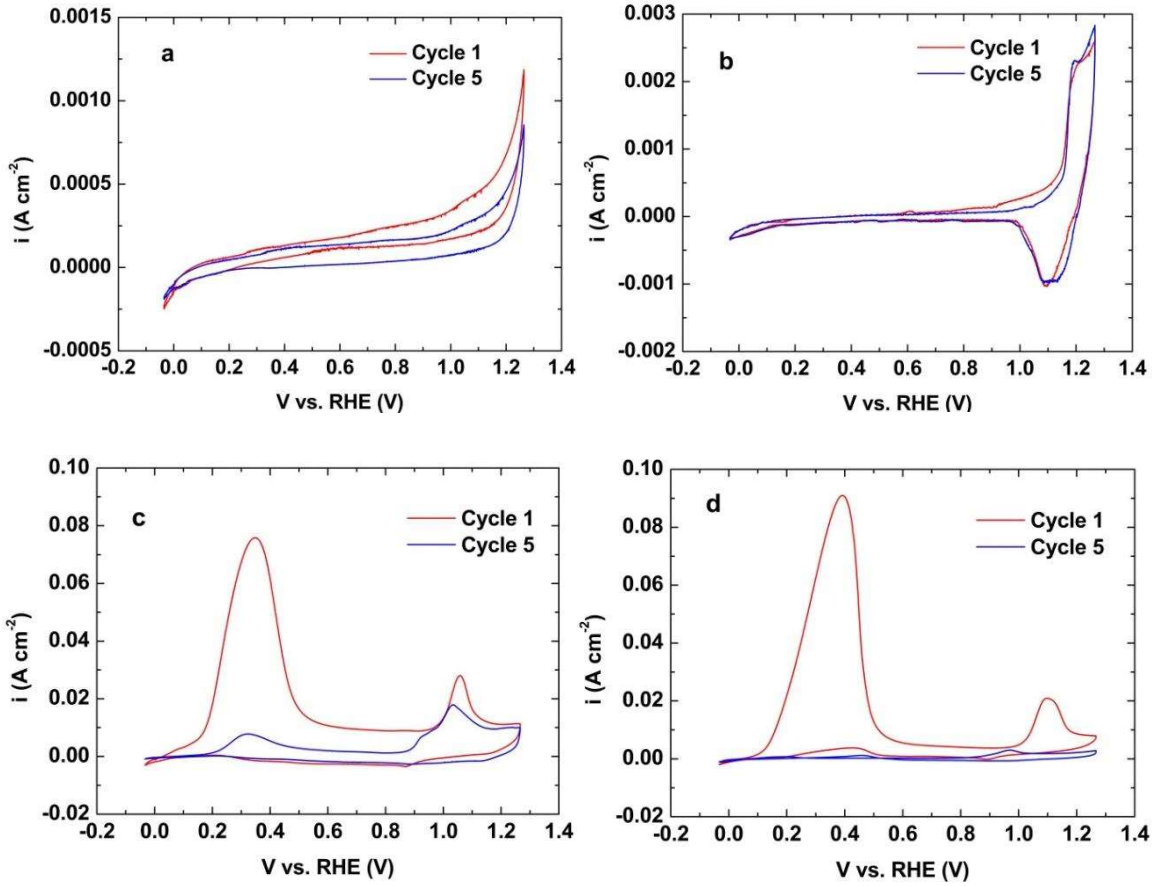

Figure 5. CVs of Co0.00 (a), Co32.45 (b), Co94.73 (c), and Co100.00 (d) electrodes in 30% w/w KOH aqueous solution with a scan rate of 5 mVs^{-1}.

The electrochemical characterization was performed by CV, at 0.005 Vs^{-1} scan rate in the potential interval between -0.035 and 1.265 V vs. RHE. At the lower and upper limits of the scanned range, HER and OER occur, respectively. In Figure 5, the first and the fifth cycles were showed for each electrode. Fig. 5(a) showed the behaviour of the Ni pure electrode. In the scanned potential range, no one peak is present, except for a small wave in the anodic scan at the potential of 1.05 V vs. RHE, that is attributed to the oxidation of Ni^{2+} to Ni^{3+} [54]. As reported in [24] in the same condition a CV of Ni strip shows a significant decrease in current density, this was attributable to the difference on the electrochemically active surface area between the two

electrodes. In particular we have esteemed that the real Ni NWs surface area is about two order of magnitude higher than planar electrode.

In Fig. 5(b), the CV of Co32.45 is shown, where the oxidation and reduction peaks of Co^{2+} / Co^{3+} are present at 1.18 V vs. RHE and 1.1 V vs RHE, respectively, according to data reported in [23]. In the region between 0.3 and 0.4 V vs. RHE, the oxidation peak due to Co to Co^{2+} was not revealed. This peak is instead visible in Figs. 5(c) and 5(d), where the CVs of Co94.73 and Co100.00, respectively, are shown. The intensity of the current related to this peak, is directly dependent on the Co content in the electrode. In fact, it reached a maximum value for the pure Co electrode and it appeared in the electrodes with a Co content higher than 85.06%.

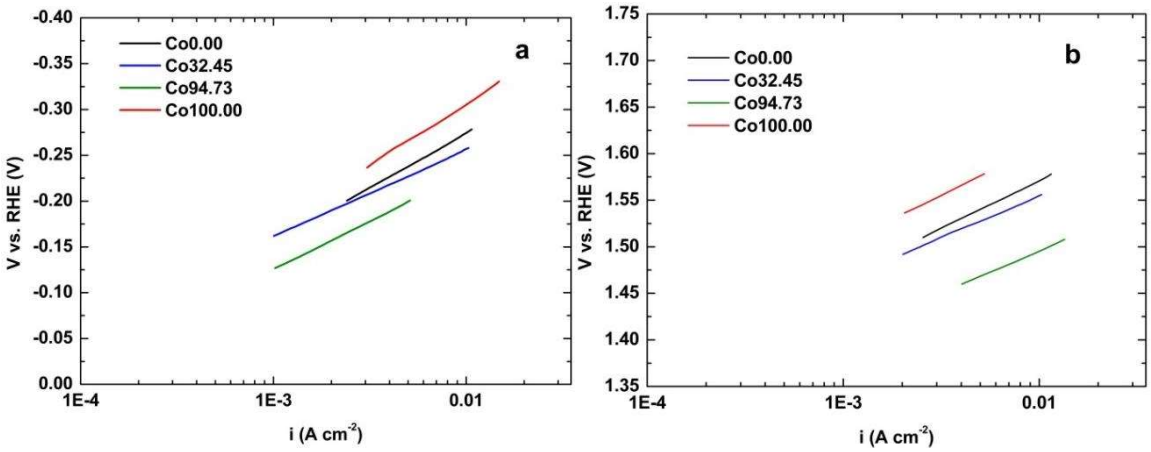

Figure 6. Linearity range of (a) cathodic QSSP for HER and (b) anodic QSSP for OER at -0.1667 mVs^{-1} scan rate in 30% w/w KOH aqueous solution at room temperature.

In order to evaluate the electrocatalytic behaviour of electrodes, QSSP tests were carried out both for HER and OER. The scanned potential range was 1 V at scan rate of 0.1667 mVs^{-1}; for HER the potential range was scanned from 0.1 V to -0.9 V vs. RHE, while for OER it was scanned from 1.1 V to 2.1 V vs. RHE.

In Figure 6, the linearity range of overpotential on logarithmic current density (reported in absolute value) is shown. In particular, Figure 6(a) shows the cathodic QSSP, while in Figure 6(b), the anodic QSSP is shown. For an exact evaluation of the experimental curves slope, they were fitted by Tafel's equation

$$\eta = a + b \log i \qquad (1)$$

where a and b parameters are respectively related to exchange current density and the slope of the Tafel's curves. In particular, $a = \frac{-2.303\mathrm{RT}}{\alpha \mathrm{zF}} log i_0$, where z is the electro-chemical equivalent of the reaction and F is the Faraday's constant.

In Table 2, the value of a and b parameters are reported. Both pure electrodes of Ni and Co have the higher slope compared to alloy electrodes. Given that the lower the value of the parameter b (in absolute value) the better the electrocatalytic performances are, we can conclude that NiCo alloys have the best electrocatalytic behaviour for the HER. In particular in the case of Co94.37 electrodes, at the same current density, a lower overpotential in absolute value with respect to the thermodynamic value of HER (0 V vs. RHE) was measured. Thus, we conclude that these types of electrodes show the best performance. The value of the slope for nanostructured electrode of pure Ni and Co agree with data reported in [8]. For OER, Figure 6(b), the pure electrodes have a similar slope, but in the case of pure Co electrodes (Co100.0) a minor overpotential was measured. From Figure 6(b) and the data reported in Table 2, it is clear that nanostructured electrodes richer in Co (Co94.73) have the best performance also for the OER. The values of b parameter relative to pure electrodes for OER agree with [8].

From these results, it can be concluded that the nanostructured electrodes made of alloy nanowires with a composition of about 95% in Co and 5% in Ni are the best performing electrocatalysts for both HER and for OER. Considering that for all electrodes, the slope of Tafel curve is close to -0.120 for HER it can be concluded that the Volmer step is the rate determining

step [52]. Besides, as we have reported in [39] the Tafel slope value for Ni strip is 0.257 V/decade, higher then value calculated for the electrodes here tested, indicating how the nanostructures lowered reaction overpotential. In the case of OER a Tafel slope of about 120 V/dec in attributable to reaction of divalent nickel or cobalt site [55]. HER and OER η_{10} potential values were also measured founding -0.231 V (RHE) and 1.494 V(RHE) respectively.

Table 2. Fitted Tafel parameters for HER and OER

	HER			OER		
Electrode	a (V)	b (V/dec)	R^2 (%)	a (V)	b (V/dec)	R^2 (%)
Co0.00	-0.511	-0.119	99.97	1.774	0.102	99.98
Co32.45	-0.444	-0.094	99.98	1.732	0.089	99.94
Co94.73	-0.441	-0.105	99.98	1.677	0.088	99.95
Co100.00	-0.571	-0.133	99.89	1.816	0.104	99.97

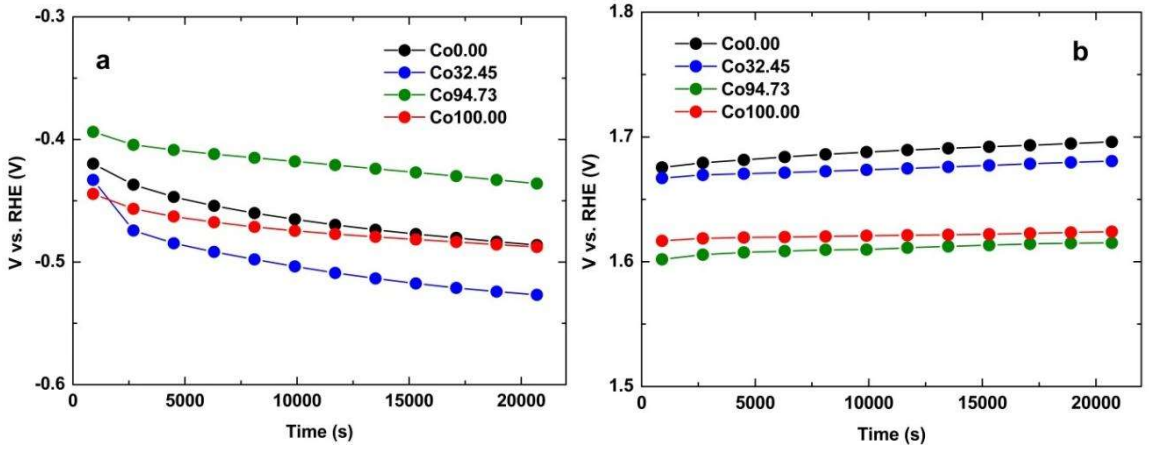

Figure 7. Constant current density mid-term stability test for (a) HER at -50 $mAcm^{-2}$ and (b) OER at 50 $mAcm^{-2}$ in 30% w/w KOH aqueous solution at room temperature.

Furthermore, constant current density tests were conducted to evaluate the mid-term behaviour of the electrodes in 30% w/w KOH solution at room temperature. In Figure 7, the electrode potential for the HER (a) and OER (b) as a function of time are shown at the applied current

density of -50 and 50 $mAcm^{-2}$, respectively, for 6 hours. Each point in the plot is the mean potential value after 1800 s.

From these tests, it can be concluded that the electrodes with the best performance are those richer in Co (Co94.73), both in terms of potential value and time stability. In fact, for the HER (Figure 7(a)) the potential decrease is 40 mV, from -0.39 V to -0.43 V vs. RHE. The same decrease was recorded for the Co100.00 electrode, from -0.44 V to -0.48 V vs. RHE. The losses are greater instead for the Co0.00 and Co 32.45 electrodes, 60 mV and 90 mV, respectively. As reported in [56], alloy with higher concentration of Co have the better catalytic activity toward the HER that can be imputable to the high hydrogen adsorption of Co. While the presence of Ni ensures low hydrogen over-potential.

In the case of OER, all electrodes have a better stability over time than the HER. In fact, the minor increase in potential was marked by the Co100.00 electrode which was 10 mV, from 1.615 V to 1.625 V vs. RHE; while the major was recorded by the Co0.00 electrode which was 20 mV, from 1.675 V to 1.695 V vs RHE. Also in this case, Co94.73 is the electrode with the best performance with an electrode potential of 1.615 V vs. RHE after 6 hours. This behaviour, as reported in [57], can be attributable to the nanocristalline/amorphous structure of this alloy that ensures abundant defect sites for oxygen evolution.

Considering the above results, the Co94.73 electrodes have the best performances both in the electrocatalytic and galvanostatic tests, besides showing a significant improvement compared to the pure Ni and Co electrodes.

In Table 3, to reassume our results and to better compare with others, the more relevant and recent literature data were listed. It can be observed that our results are very close to that obtained from others authors.

Table 3. Comparison of performance of various electrocatalysts (TW: this work)

Electrocatalysts	Reaction	KOH solution	Tafel slope (mV/dec)	Current density (mA/cm^2)	Potential at current density (V vs. RHE)	Ref.
Ni strip	HER	30 % w/w	-142			[58]
Ni NWs	HER	30 % w/w	-118	-10	-0.250	[58]
Ni NWs + Pd NPs	HER	30 % w/w	-120			[58]
$Ni_{0.95}Dy_{0.05}$	HER	8 M	-101	-10	-0.240	[59]
CoP/CC	HER	1 M	-129	-10	-0.209	[60]
Ni_2P@mesoG	HER	1 M	-99	-10	-0.188	[61]
Petaloid FeP/C	HER	1 M	-93	-10	-0.185	[62]
NiW 1:1	HER	6 M	-112			[63]
PTFE Ni-Raney	HER	38 % w/w	-111	-10	-0.208	[64]
3D Ni Foam	HER	8 M	-105	-10	-0.200	[65]
FeNiP-S/NF-5	HER	1 M	-104.5	-20	-0.183	[66]
FeSe-NF	HER	1 M	-145	-10	-0.200	[67]
CoP/rGO/NF-3	HER	1 M	-135			[68]
Ni NWs	HER	30 % w/w	-119	-10	-0.275	TW
$Ni_{68}Co_{32}$ NWs	HER	30 % w/w	-94	-10	-0.256	TW
Ni_6Co_{94} NWs	HER	30 % w/w	-105	-10	-0.231	TW
FeSe-NF	OER	1 M	109			[67]
Co@C	OER	1 M	109	10	1.599	[69]
Co-NiSe-2	OER	1 M	110	100	1.61	[70]
MOF [Cu(OH)2]/CF	OER	1 M	108	10	1.56	[71]
$Ni_{2.85}Fe_{0.15}(NO_3)_2(OH)_4$	OER	1M	121	10	1.51	[72]
1-RuO2/CeO2	OER	1 M	74	10	1.58	[73]
PO-Ni/Ni-N-CNFs	OER	1 M	113	10	1.65	[74]
CNF@C	OER	1 M	141	10	1.544	[75]
Ni NWs	OER	30 % w/w	102	10	1.57	TW
$Ni_{68}Co_{32}$ NWs	OER	30 % w/w	89	10	1.554	TW
Ni_6Co_{94} NWs	OER	30 % w/w	88	10	1.501	TW

In Figure 8 the SEM images of electrode after constant current density mid-term stability were reported. The morphology of the nanowires is practically unchanged compared to Figure 4, referred to the nanowires immediately after preparation. This explains the catalytic stability of the electrodes. A thin patina is present on the top of some of them. From the EDS analysis made on these samples (Figure S2), we think that this patina is due to the formation of a thin layer of KOH which is formed by precipitation on the electrode when it is disassembled from the electrolysis cell and following drying in the air.

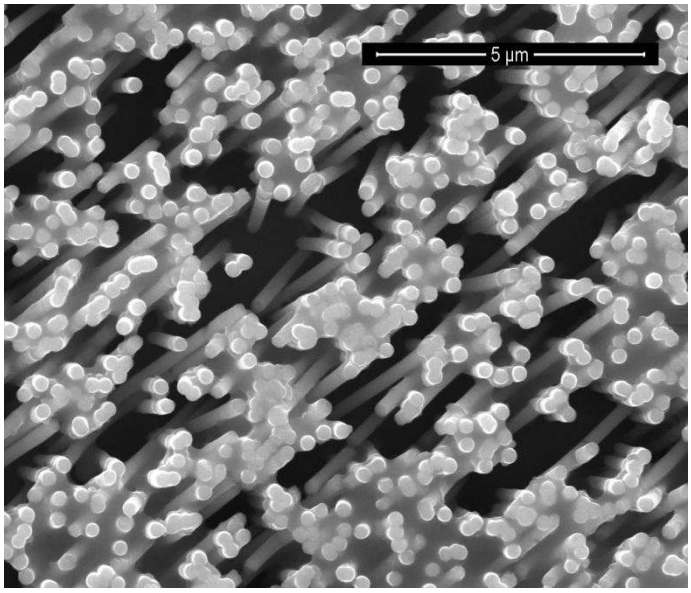

Figure 8. SEM images of nanowires after mid-term stability at 50 $mAcm^{-2}$ in 30% w/w KOH aqueous solution at room temperature.

CONCLUSION

Nanostructured electrodes of Ni-Co alloys were fabricated with the simple and cheap method of template electrosynthesis. These electrodes were investigated both as a cathode and anode for the water splitting reaction in an aqueous solution of 30% w/w KOH at room temperature. For the alloy electrodeposition, various mixtures of concentrated solutions of Ni and Co with different volume ratios were used in order to obtain alloys with different composition. After the template dissolution, a chemical characterization was carried out by EDS to evaluate the atomic composition of the obtained samples, followed by a SEM morphological characterization. From the results of the EDS analysis, it was found that the atomic composition of Co is higher than Ni. Also the NWs composition are richer in Co than the Co solution concentrations used for the deposition nanowires. This behaviour was attributed to the presence of boric acid in the deposition solution that formed with Ni a complex more stable in comparison to that one with Co one.

Electrochemical and electrocatalytic characterizations were carried out through CV and QSSP respectively. In particular, results of both cathodic and anodic QSSPs have shown that the electrodes with a Co atomic composition of about 95% have the best performances for both HER and OER. In addition, galvanostatic tests were carried out at both constant cathodic and anodic current densities of 0.05 Acm^{-2} intensity for 6 hours to verify mid-term behaviour. All electrodes have been particularly stable for the OER. Furthermore, even in these tests, the Co94.73 electrodes showed a better behaviour both for the HER and the OER.

Further research activities are in progress for tests at different temperatures, with forced convection and the coupling of cathode and anode of nanostructured alloys in a single cell.

REFERENCES

1. Jacobson MZ, Delucchi MA, Bauer ZAF, Goodman SC, Chapman WE, Cameron et al. 100% Clean and Renewable Wind, Water, and Sunlight All-Sector Energy Roadmaps for 139 Countries of the World. Joule. 2017;1:108-21.
2. Chu S, Majumdar A. Opportunities and challenges for a sustainable energy future. Nature. 2012;488:294-303.
3. Bocci E, Zuccari F, Dell'Era A. Renewable and hydrogen energy integrated house. Int J Hydrog Energy. 2011;36:7963-68.
4. Yilmaz F, Balta MT, Selbas R. A review of solar based hydrogen production methods. Renew and Sustainable Energy Rev. 2016;56:171-8.
5. Rodriguez CA, Modestino MA, Psaltis D, Moser C. Design and cost considerations for practical solar-hydrogen generators. Energy Environ Sci. 2014;7:3828-35.
6. Holladay JD, Hu J, King DL, Wang Y. An overview of hydrogen production technologies. Catalysis Today. 2009;139:244-60.
7. Schmidt O. Gambhir A, Staffell I, Hawkes A, Nelson J, Few S. Future cost and performance of water electrolysis: An expert elicitation study. Int J Hydrog Energy. 2017;42:30470-92.
8. Zeng K, Zhang, D. Recent progress in alkaline water electrolysis for hydrogen production and applications. Prog Energy Combust Sci. 2010;36(3):307-26.

9. Zhang X, Chan SH, Ho HK, Tan SC, Li M, Li G, Li J, Feng Z. Towards a smart energy network: The roles of fuel/electrolysis cells and technological perspectives. Int J Hydrog Energy. 2015;40:6866-919.
10. Marcelo D, Dell'Era A. Economical electrolyser solution. Int J Hydrog Energy. 2008;33:3041-4.
11. Sapountzi FM, Gracia JM, Weststrate CJ, Fredriksson HOA, Niemantsverdriet JW. Electrocatalysts for the generation of hydrogen, oxygen and synthesis gas. Prog Energy Combust Sci. 2017;58:1-35.
12. Lyons MEG, Brandon, MP. A comparative study of the oxygen evolution reaction on oxidised nickel, cobalt and iron electrodes in base. J Ele Chem. 2010;641:119-30.
13. Goswami C, Hazarika KK, Bharali P. Transition metal oxide nanocatalysts for oxygen reduction reaction. Materials Science for Energy Technologies. 2018;1:117-28.
14. Bockris JOM, Reddy AKN, Gamboa-Aldeco M. Modern Electrochemistry. 2nd ed. New York: Kluwer Academic, Plenum Publishers; 2000.
15. Zhang Y, Cao X, Yuan H, Zhang W, Zhou Z. Oxygen evolution reaction on Ni hydroxide film electrode containing various content of Co. Int J Hydrog Energy. 1999;24:529-536.
16. Trzesniewski BJ, Diaz-Morales O, Vermaas DA, Longo A, Bras W, Koper MTM, Smith WA. In situ observation of active oxygen species in Fe-containing Ni-based oxygen evolution catalysts: the effect of pH on electrochemical activity. J Am Chem Soc. 2015;137:15112-21.
17. Cheng Y, Liu C, Cheng HM, Jiang SP. One-Pot Synthesis of Metal–Carbon Nanotubes Network Hybrids as Highly Efficient Catalysts for Oxygen Evolution Reaction of Water Splitting. ACS Appl Mater Interfaces. 2014;6:10089-98.
18. Cheng, Y, Jiang SP. Advances in electrocatalysts for oxygen evolution reaction of water electrolysis-from metal oxides to carbon nanotubes. Progress in Natural Science: Materials International. 2015;25(6):545-53.
19. Zhu J, Li H, Zhong L, Xiao P, Xu X, Yang X, et al. Perovskite oxides: preparation, characterizations and applications in heterogeneous catalysis. ACS Catal. 2014;4:2917-40.
20. Gong M, Wang DY, Chen CC, Hwang BJ, Dai H. A mini review on nickel-based electrocatalysts for alkaline hydrogen evolution reaction. Nano Research. 2016;9:28-46.
21. Safizadeh F, Ghali E, Houlachi G. Electrocatalysis developments for hydrogen evolution reaction in alkaline solutions – A Review. Int J Hydrog Energy. 2015;40:256-74.
22. Hall DS, Bock C, MacDougall BR. The electrochemistry of metallic nickel: oxides, hydroxides, hydrides and alkaline hydrogen evolution. J Electrochem Soc. 2013;160:235-43.

23. Pérez-Alonso FJ, Adán C, Rojas S, Peña MA, Fierro JLG. Ni-Co electrodes prepared by electroless-plating deposition. A study of their electrocatalytic activity for the hydrogen and oxygen evolution reactions. Int J Hydrog Energy. 2015;40:51-61.
24. Ganci F, Lombardo S, Sunseri C, Inguanta R. Nanostructured electrodes for hydrogen production in alkaline electrolyzer. Renewable Energy. 2018;123:117-24.
25. Shviro M, Polani S, Dunin-Borkowski RE, Zitoun D. Bifunctional Electrocatalysis on Pd-Ni Core–Shell Nanoparticles for Hydrogen Oxidation Reaction in Alkaline Medium. Adv Mater Interfaces. 2018;1701666.
26. Hong SH, Ahn SH, Choi I, Pyo SG, Kim HJ, Jang JH, Kim SK. Fabrication and evaluation of nickel cobalt alloy electrocatalysts for alkaline water splitting. Appl Surf Sci. 2014;307:146-52.
27. Povroznik VS, Shein AB, Mikova IN. Effect of anodic surface treatment of cobalt silicides on the hydrogen evolution reaction. Prot Met. 2008;44:557-60.
28. Shalom M, Ressnig D, Yang X, Clavel G, Fellinger TP, Antonietti M. Nickel nitride as an efficient electrocatalyst for water splitting. J Mater Chem A. 2015;3:8171-7.
29. Karimzadeh A, Aliofkhazraei M, Walsh FC. A review of electrodeposited Ni-Co alloy and composite coatings: Microstructure, properties and applications. Surf Coat Tech. 2019;372:463-498.
30. Mistry H, Varela AS, Kühl S, Strasser P, Cuenya BR. Nanostructured electrocatalysts with tunable activity and selectivity. Nature Rewiev. 2016;1:16009.
31. Ahn SH, Choi I, Park HY, Hwang SJ, Yoo SJ, Cho E, Kim HJ, Henkensmeier D, Nam SW, Kim SK, Jang JH. Effect of morphology of electrodeposited Ni catalysts on the behavior of bubbles generated during the oxygen evolution reaction in alkaline water electrolysis. Chem Commu. 2013;43:9323-5.
32. Wang HY, Hsu YY, Chen R, Chan TS, Chen HM, Liu B. Ni^{3+} induced formation of active NiOOH on the spinel Ni-Co oxide surface for efficient oxygen evolution reaction. Adv Energy Mater. 2015;5:1500091.
33. Lu X, Liu J, Li Y, Li Y, Sun X. Au/NiCo2O4 arrays with high activity for water oxidation. Chem Cat Chem. 2014;6:2501-6.
34. Cui B, Lin H, Li J, Li X, Yang J, Tao J. Core-ring structured $NiCo_2O_4$ nanoplatelets: synthesis, characterization and electrocatalytic applications. Adv Funct Mater. 2008;15:1440-7.

35. Pierozynski B, Mikolajczyk T, Kowalski IM. Hydrogen evolution at catalytically- modified nickel foam in alkaline solution. J Power Sources. 2014;271:231-8.
36. Zhang L, Xiong K, Chen S, Li L, Deng Z, Wei Z. In situ growth of ruthenium oxide-nickel oxide nanorod arrays on nickel foam as a binder-free integrated cathode for hydrogen evolution. J Power Sources. 2015;274:114-120.
37. Barati Darband G, Aliofkhazraei M, Sabour Rouhaghdam A. Facile electrodeposition of ternary Ni-Fe-Co alloy nanostructure as a binder free, cost-effective and durable electrocatalyst for high-performance overall water splitting. J Colloid Interf Sci. 2019;547;407-420.
38. Barati Darband G, Aliofkhazraei M, Hyun S, Sabour Rouhaghdam A, Shanmugam S. Electrodeposited NiCoP hierarchical nanostructure as a cost-effective and durable electrocatalyst with superior activity for bifunctional water splitting. J Power Sources. 2019;429:156-167.
39. Ganci F, Cusumano V, Sunseri C, Inguanta R. Performance Enhancement of Alkaline Water Electrolyzer Using Nanostructured Electrodes Synthetized by Template Electrosynthesis. IEEE 4th International Forum on Research and Technology for Society and Industry (RTSI). 2018.
40. Battaglia M, Inguanta R, Piazza S, Sunseri C. Fabrication and characterization of nanostructured Ni-IrO_2 electrodes for water electrolysis. Int J Hydrog Energy. 2014;39:16797-805.
41. Ganci F, Inguanta R, Piazza S, Sunseri C, Lombardo S. Fabrication and Characterization of Nanostructured Ni and Pd Electrodes for Hydrogen Evolution Reaction in Water Alkaline Electrolyzer. Chem Eng Trans. 2017;57:1591-6.
42. Inguanta R, Piazza S, Sunseri C. Synthesis of self-standing Pd nanowires via galvanic displacement deposition. Electrochemistry Communications. 2009;11:1385-8.
43. Lupi C, Dell'Era A, Pasquali M. Nickel–cobalt electrodeposited alloys for hydrogen evolution in alkaline media. Int J Hydrog Energy. 2009;34:2101-6.
44. Burzyńska L, Rudnik E. The influence of electrolysis parameters on the composition and morphology of Co–Ni alloys. Hydrometallurgy. 2000;54:133-49.
45. Graff A, Barre E, Baranek P, Bachet M, Benezeth P. Complexation of Nickel Ions by Boric Acid or (Poly)borates. J Solution Chem. 2017;46:25-43.
46. Bousher A. Review: unidentate complexes involving borate. J Coordination Chem. 1995;34:1-11.

47. Schweckandt DS, Aguirre MC. Electrodeposition of Ni-Co alloys. Determination of properties to be used as coins. Procedia Mat Sci. 2015;8:91-100.
48. Silipigni L, Barreca F, Fazio E, Neri F, Spanò T, Piazza S, Sunseri C, Inguanta R. Template Electrochemical Growth and Properties of Mo Oxide Nanostructures. J Physical Chem C. 2014;118:22299-308.
49. Maksimović VM, Lačnjevac UČ, Stoiljković MM, Pavlović MG, Jović VD. Morphology and composition of Ni–Co electrodeposited powders, Materials Characterization. 2011;62:1173-9.
50. Mukhtar A, Mehmood T, Wu KM. Investigation of phase transformation of CoNi alloy nanowires at high potential. IOP Conference Series: Materials Science and Engineering. 239:1.
51. Lu W, Liebscher CH, Dehm G, Raabe D, Li Z. Bidirectional Transformation Enables Hierarchical Nanolaminate Dual-Phase High-Entropy Alloys. Adv Mat. 2018:30; 1804727.
52. Barati Darband G, Aliofkhazraei M, Shanmugam S. Recent advances in methods and technologies for enhancing bubble detachment during electrochemical water splitting. Renew Sust Energ Rev. 2019;114:109300.
53. Wen R, Xu S, Ma X, Lee YC, Yang R. Three-Dimensional Superhydrophobic Nanowire Networks for Enhancing Condensation Heat Transfer. Joule. 2018;2:269-79.
54. Lian K, Birss VI. Hydrous Oxide Film Growth on Amorphous Ni-Co Alloys. J Electrochem Soc. 1991;138:2877-84.
55. Kinoshita K. Electrochemical Oxygen Technology. New York: Wiley; 1992.
56. Grubac Z, Sesar A. Electrocatalytic Activity of the Ni57.3Co42.7 Alloy for the Hydrogen Evolution. Croat Chem Acta. 2017;90(2):273-80.
57. Yang Y, Fei H, Ruan G, Xiang C, Tour JM. Efficient Electrocatalytic Oxygen Evolution on Amorphous Nickel–Cobalt Binary Oxide Nanoporous Layers. ACS Nano. 2014;8(9):9518-23.
58. Ganci F, Baguet T, Aiello G, Cusumano V, Mandin P, Sunseri C, Inguanta R. Nanostructured Ni Based Anode and Cathode for Alkaline Water Electrolyzers. Energies. 2019;12:3669.
59. Cardoso DSP, Amaral L, Santos DMF, Sljuki B, Sequeira CAC, Macci D, Saccone A. Enhancement of Hydrogen Evolution in Alkaline Water Electrolysis by using Nickel-Rare Earth Alloys. Int J Hydrog Energy. 2015;40:4295-302.
60. Tian J, Liu Q, Asiri AM, Sun X. Self-Supported Nanoporous Cobalt Phosphide Nanowire Arrays: An Efficient 3D Hydrogen-Evolving Cathode over the Wide Range of pH 0−14. J Am Chem Soc. 2014;136:7587-90.

61. Jeoung S, Seo B, Hwang JM, Joo SH, Moon HR. Direct Conversion of Coordination Compounds into Ni_2P Nanoparticles Entrapped in 3D Mesoporous Graphene for an Efficient Hydrogen Evolution Reaction. Mater Chem Front. 2017;1:973-8.
62. Wang F, Yang X, Dong B, Yu X, Xue H, Feng L. A FeP Powder Electrocatalyst for the Hydrogen Evolution Reaction. Electrochem commun. 2018;92:33-8.
63. Tasić GS, Lačnjevac U, Tasić MM, Kaninski MM, Nikolić VM, Žugić DL, Jović VD. Influence of Electrodeposition Parameters of Ni–W on Ni Cathode for Alkaline Water Electrolyser. Int J Hydrog Energy. 2013;38(11):4291-7.
64. Salvi P, Nelli P, Villa M, Kiros Y, Zangari G, Bruni G, Marini A, Milanese C. Hydrogen Evolution Reaction in PTFE Bonded Raney-Ni Electrodes. Int J Hydrog Energy. 2011;36(13):7816-21.
65. Siwek KI, Eugénio S, Santos DMF, Silva MT, Montemor MF. 3D Nickel Foams with Controlled Morphologies for Hydrogen Evolution Reaction in Highly Alkaline Media. Int J Hydrog Energy. 2019;44(3):1701-9.
66. Li H, Du Y, Pan L, Wu C, Xiao Z, Liu Y, Sun X, Wang L. Ni Foil Supported FeNiP Nanosheet Coupled with NiS as Highly Efficient Electrocatalysts for Hydrogen Evolution Reaction. Int J Hydrog Energy.2020. https://doi.org/10.1016/j.ijhydene.2020.06.268
67. Chanda D, Tufa RA, Birdja YY, Basu S, Liu S. Hydrothermally/Electrochemically Decorated FeSe on Ni-Foam Electrode: An Efficient Bifunctional Electrocatalysts for Overall Water Splitting in an Alkaline Medium. Int J Hydrog Energy. 2020. https://doi.org/10.1016/j.ijhydene.2020.07.055
68. Yang Z, He R, Wu H, Ding Y, Mei H. Needle-like CoP/rGO Growth on Nickel Foam as an Efficient Electrocatalyst for Hydrogen Evolution Reaction. Int J Hydrog Energy. 2020. https://doi.org/10.1016/j.ijhydene.2020.07.114
69. Wu Q, Li T, Wang W, XiaoY. High-Throughput Chainmail Catalyst FeCo@C Nanoparticle for Oxygen Evolution Reaction. Int J Hydrog Energy. 2020. https://doi.org/10.1016/j.ijhydene.2020.07.051
70. Liang D, Mao J, Liu P, Li J, Yan J, Song W. In-Situ Doping of Co in Nickel Selenide Nanoflower for Robust Electrocatalysis Towards Oxygen Evolution. Int J Hydrog Energy. 2020. https://doi.org/10.1016/j.ijhydene.2020.07.017
71. Li H, Liu Y, He F, Yang H, Li Z, Zhou Q, Tang K. In Situ Grown Cu-Based Metal-Organic Framework on Copper Foam as High-Performance Electrocatalysts for Oxygen Evolution Reaction. Int J Hydrog Energy.2020;45(41):21540-6.

72. Liu Y, Han N, Jiang J, Ai L. Boosting the Oxygen Evolution Electrocatalysis of Layered Nickel Hydroxidenitrate Nanosheets by Iron Doping. Int J Hydrog Energy. 2019;44(21):10627-36.
73. Galani SM, Mondal A, Srivastava DN, Panda AB. Development of RuO_2/CeO_2 Heterostructure as an Efficient OER Electrocatalyst for Alkaline Water Splitting. Int J Hydrog Energy. 2020;45(37):18635-44.
74. Wu ZY, Ji WB, Hu BC, Liang HW, Xu XX, Yu ZL, Li BY, Yu SH. Partially Oxidized Ni Nanoparticles Supported on Ni-N co-Doped Carbon Nanofibers as Bifunctional Electrocatalysts for Overall Water Splitting. Nano Energy. 2018;51:286-93.
75. Cao GL, Yan YM, Liu T, Rooney D, Guo YF, Sun KN. Three-Dimensional Porous Carbon Nanofiber Networks Decorated with Cobalt-Based Nanoparticles: A Robust Electrocatalyst for Efficient Water Oxidation. Carbon. 2015;94:680-6.

Supplementary Material

Click here to download Supplementary Material: SupplementaryMaterial.docx

***Declaration of Interest Statement**

Declaration of interests

☒ The authors declare that they have no known competing financial interests or personal relationships that could have appeared to influence the work reported in this paper.

☐The authors declare the following financial interests/personal relationships which may be considered as potential competing interests: